Materials Letters 128 (2014) 421–424

Contents lists available at ScienceDirect

Materials Letters

journal homepage: www.elsevier.com/locate/matlet

# Molten salt synthesis of potassium-containing hydroxyapatite microparticles used as protein substrate

Nikolas T. Weissmueller [a,b,c,*], Heiko A. Schiffter [b], Andrew J. Pollard [a,c], A. Cuneyt Tas [d]

[a] Oxford Vaccine Group, Department of Paediatrics, University of Oxford and the NIHR Oxford Biomedical Research Institute, Oxford OX3 7LE, United Kingdom
[b] Biomedical Ultrasonics, Biotherapy & Biopharmaceuticals Laboratory, University of Oxford, Oxford OX3 7DQ, United Kingdom
[c] The Oxford Martin School, University of Oxford, Old Indian Institute, Oxford OX1 3BD, United Kingdom
[d] Department of Materials Science and Engineering, University of Illinois, Urbana, IL 61801, USA

ARTICLE INFO

*Article history:*
Received 8 July 2013
Accepted 22 April 2014
Available online 29 April 2014

*Keywords:*
Hydroxyapatite
Biomaterial
Molten salt synthesis
Bovine serum albumin
Adsorption

ABSTRACT

The bioactivity of a material may be favorably altered by exerting control over its protein sorption propensity. Spheroidal potassium-containing calcium phosphate bioceramic microparticles were manufactured by molten salt synthesis. The effects on particle characteristics and adsorption of bovine serum albumin (BSA) of different hydroxyapatite (HA, $Ca_{10}(PO_4)_6(OH)_2$) to salt flux ($K_2SO_4$) ratios were investigated. X-ray diffraction (XRD) patterns showed the emergence of minor phases in addition to the HA major phase with increased salt flux. Synthesized particles were found to increase in potassium content with increasing HA:$K_2SO_4$ ratio. Conversely, the amount of BSA adsorption onto microparticles, normalized for surface area, decreased with excess $K_2SO_4$. The results indicate that $K_2SO_4$ content can impact the morphology, composition, and BSA adsorption propensity of the resultant bioceramic microparticles.



## 1. Introduction

The ability to control the physical properties of inorganic crystals is an important aim of materials science. Crystal composition, size, and morphology can significantly alter the protein adsorption propensity of an inorganic material and thereby impact its bioactivity [1–3]. Therefore, the control over protein sorption via the design of material properties may be used to favorably alter the bioactivity of a material. In the case of hydroxyapatite (HA, $Ca_{10}(PO_4)_6(OH)_2$), a biocompatible ceramic with osteo-conductive properties that is routinely used in the structural repair of bone and dental defects [4,5], the protein adsorption behavior can be substantially altered depending on which crystal surface is exposed to the aqueous milieu [6]. Acidic proteins were described to preferentially adsorb to the positively charged calcium ions present on the *a*(*b*)-planes, while basic proteins preferentially adsorb to the hydroxyl groups present on the *c*-planes of HA crystals [6]. Ionic substitutions in the HA crystal lattice can further alter protein adsorption properties [7]. Molten salt synthesis (MSS) is reportedly one of the simplest methods to manufacture single HA crystals with platelet, needle, or whisker morphologies [8]. While cationically doped HA crystals of various morphologies have been synthesized, this is the first report to describe MSS of spheroidal potassium-substituted HA crystals and their protein adsorption propensity.

## 2. Materials and methods

*Synthesis and characterization of spheroidal potassium-substituted HA crystals*: HA powder ($Ca_{10}(PO_4)_6(OH)_2$, Sigma 13204, UK) was mixed with potassium sulfate salt ($K_2SO_4$, Sigma P0772, UK) in HA:$K_2SO_4$ ratios 1:3, 1:6, and 1:9 by weight. The ball-milled powders were heated at 5 °C/min and fluxed in covered high alumina crucibles (Coors–Sigma Z247642, UK) at 1200 °C for 3.5 h before cooling to room temperature at 5 °C/min. The $K_2SO_4$ flux was removed by washing with hot deionized water. The products were characterized by using X-ray diffraction (XRD, Bruker D5000, Ettlingen, Germany), energy dispersive X-ray spectrometry (EDS, JEOL 840A, Herts, UK), static light scattering (MasterSizer S, Malvern, Worcestershire, UK), helium pycnometry (Pyc-nomatic ATC, ThermoFisher, Loughborough, UK), dynamic light scattering (Zetasizer Nano ZS, Malvern, Worcestershire, UK), and atomic absorption spectroscopy (AAS, Varian AA240, Agilent Inc., Wokingham, UK). X-ray diffraction analysis used copper Kα radiation ($\lambda = 0.15406$ nm) and a scan rate of 0.04°/s $2\theta$. Phases were identified by comparison to the International Centre for Diffraction Data-Powder Diffraction File (ICDD-PDF) database. Particle morphology was assessed by scanning electron microscopy (SEM, Amray 1810T, Bedford, MA, USA). The median particle diameter (D($n$, 0.5))

* Corresponding author at: Institute of Biomedical Engineering, Old Road Campus Research Building, Oxford, OX3 7DQ, United Kingdom.
Tel.: +44 1865 617711; fax: +44 1865 617701.
*E-mail address:* nikolas.weissmueller@gmail.com (N.T. Weissmueller).

http://dx.doi.org/10.1016/j.matlet.2014.04.154
0167-577X/

and the span=([D(*n*,0.9)-D(*n*,0.1)]/D(*n*,0.5)) of the respective particle number distribution was determined by He–Ne laser light scattering. He–Ne laser refractive measurements used *RI*=1.651 for bioceramics dispersed in deionized water (*RI* 1.330). The specific surface area (SSA) was determined from light scattering data and particle density according to Mie theory. Zeta potentials were determined at 1 mg/mL powder in potassium-buffered saline pH 7.4 (*RI*=1.332) (PBS, Sigma P4417) based on Smoluchowski equation according to the manufacturer's instructions.

*BSA adsorption and quantification*: Powder samples of 10 mg each were incubated at room temperature (RT) for 2 hours with 1 mL of 5 mg/mL of bovine albumin tetramethylrhodamine isothiocyanate (BSA-TRITC, Sigma A2289, UK) in PBS pH 7.4 (PBS, Sigma P4417) on a VWR rotating shaker (VWR, Dublin, Ireland). After adsorption, the powders were washed thrice with isopropanol (Fisher Scientific, P/7507/17, UK) and dried in a desiccator. Protein loading of BSA-TRITC was assessed on dry crystals using fluorescence imaging at 80 ms exposure and 4 × magnification on Nikon Eclipse Ti and NIS Elements AR 3.0 software. Fluorescence intensity was averaged over the respective particle area as seen by the fluorescence microscope using ImageJ analysis software (available at http://rsb.info.nih.gov/ij; developed by Wayne Rasband, National Institutes of Health, Bethesda, MD, USA) and reported from low to high on a 0 and 256 bit gray scale intensity spectrum.

## 3. Results and discussion

*Powder characterization*: Scanning electron micrographs show a progressively spheroidal shape of the synthesized bioceramic microparticles as the $K_2SO_4$ flux-to-HA powder ratio increases (Fig. 1). While particle densities and specific surface area (SSA) increased with increasing salt flux, zeta potential and aspect ratios decreased (Table 1). Light scattering data suggests that the average particle diameter was less at higher salt flux ratios with size distributions encompassed by a span of 1.0–2.0. At higher $K_2SO_4$ mass, the HA concentration in the melt decreases while the distance between seed-particles in the melt increases. These two phenomena could allow for a shift from a solution-diffusion dominated process, to a solution-precipitation dominated process and may partially explain the different morphologies [9]. The mechanism of nucleation and growth of phase pure hydroxyapatite whiskers from a molten salt of potassium sulfate was previously described in detail by Tas [8] for low (i.e., 1:1.2 or 1:3) HA:$K_2SO_4$ ratios. Increasing the HA:$K_2SO_4$ ratio of the current study to 1:6 or 1:9 had a pronounced effect of manufacturing spheroidal particles with smooth, amorphous-looking surfaces, instead of obtaining high aspect ratio whiskers or particles exhibiting faceted surfaces [8]. We refer the readers to Tas [8] for a full physical chemical discussion of the formation of calcium phosphates in the molten salt synthesis technique.

XRD patterns (Fig. 2) of the as-synthesized microparticles conformed to the standard d-spacings of HA (ICDD PDF 55-0592). The unusually high peak intensities ( > 25,000 cps) registered for the 1:3 samples of Fig. 2a indicate the suitability of this process for synthesizing single crystals. In this method of synthesis, crystals of apatitic calcium phosphate are produced and the most intense XRD peak is located on the (300) plane at 32.91 2$\theta$, instead of the (211) plane. This difference is due to HA crystal orientation along the *c* axis [8,10]. As the ratio of $K_2SO_4$ to HA increases, an overall decrease in crystallinity and the emergence of additional minor mineral phases is observed. In the 1:3 condition, the observed minor phase is $Ca(PO_3)_2$ (ICDD PDF 11-0039). The 1:6 condition produced the minor phases beta-tricalcium phosphate (β-TCP, ICDD PDF 09-169) and $Ca(PO_3)_2$. β-TCP is known to be biocompatible and to enhance bioresorbability [11,12]. At a 1:9 ratio, minor phases of alpha-tricalcium phosphate ($\alpha$-$Ca_3(PO_4)_2$, ICDD PDF 09-348) and potassium-substituted calcium metaphosphate ($KCaPO_4$, ICDD PDF 33-1002) are additionally observed. It will be quite difficult, if not impossible at all, to label certain regions of particles or discrete particles depicted in Fig. 1 with different phases, such as hydroxyapatite or tricalcium phosphate, without using TEM (transmission electron microscopy). A TEM study was outside the experimental scope of this short communication.

The incorporation of potassium ions into the combined bioceramic (i.e., HA and K-phosphate phases) is confirmed by atomic absorption spectroscopy (AAS), and was observed to increase at higher salt mass (Table 1). Fig. 3a furthermore suggests that Ca/P ratio decreases with increasing potassium content (Fig. 3a). Although the substitution of potassium in lieu of calcium ions in the crystal lattice could account for this trend, more data are required to substantiate this possibility. However, the ability of cations to incorporate into aqueous apatite solutions is well known [13]. Despite the incorporation of a small amount of potassium (0.1–0.23 wt%) from the $K_2SO_4$ flux during MSS, Zhang and Zhu observed no significant morphological changes in their ~50 μm rod-like particles of fluoride-substituted HA (FHA) [14]. When they used $Na_2SO_4$ flux, however, the high incorporation of sodium cations into the apatite stunted growth and resulted in ~50 nm spheroidal FHA particles [14]. Although a direct comparison to these FHA particles is not possible, the results presented in this paper similarly suggest that potassium cations may be incorporated into the apatite phase of micron-sized particles. Our results further suggest that particle morphology, density, and SSA change as a function of excess $K_2SO_4$ flux, and that these changes are accompanied by the emergence of minor phases at the expense of particle crystallinity.

*Protein adsorption*: Adsorption of negatively charged BSA, measured by TRITC fluorescence intensity in the dry state and normalized to the imaged particle area, showed a more than 7-fold higher protein adsorption onto HA:$K_2SO_4$ (1:3) particles compared to 1:9 particles ($p < 0.001$). Mean fluorescence of the 1:3 particles was

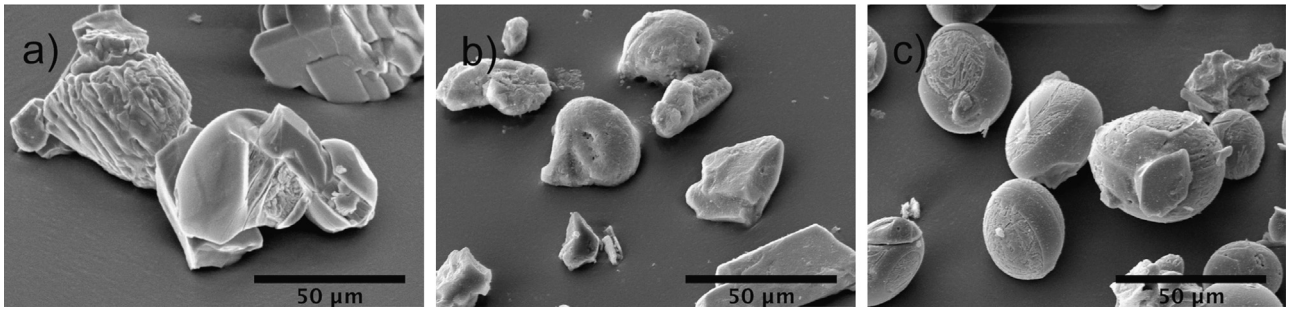


**Fig. 1.** SEM images of microparticles show (a) mixed faceted crystalline and amorphous looking-surface morphology for the HA:Flux (1:3) particles, (b) increasingly spheroidal and amorphous-looking morphology for HA:Flux (1:6), and (c) largely spheroidal particles for HA:Flux (1:9).

**Table 1**
Microparticle characteristics; reported as means ± SD ($n=3$)

| Condition HA:Salt flux | Size (μm) distribution Median (span) | Aspect ratio distribution Median (Min – Max) | Molar ratio Ca/K | Density g/cm$^3$ | ζ-potential g/cm(mV) | SSA ($m^2$/g) |
|---|---|---|---|---|---|---|
| HA:$K_2SO_4$-1:3 | 54.5 (1.2) | 1.3 (1.0–3.1) | 39.6 (±5.7) | 2.87 (±0.03) | −18.7 (±2.6) | 0.15 (±0.01) |
| HA:$K_2SO_4$-1:6 | 36.1 (2.1) | 1.2 (1.0–2.0) | 6.7 (±3.2) | 3.16 (±0.03) | −14.0 (±0.7) | 0.16 (±0.03) |
| HA:$K_2SO_4$-1:9 | 36.8 (1.4) | 1.1 (1.0–2.0) | 1.1 (±0.5) | 3.32 (±0.03) | −13.3 (±1.7) | 0.24 (±0.02) |

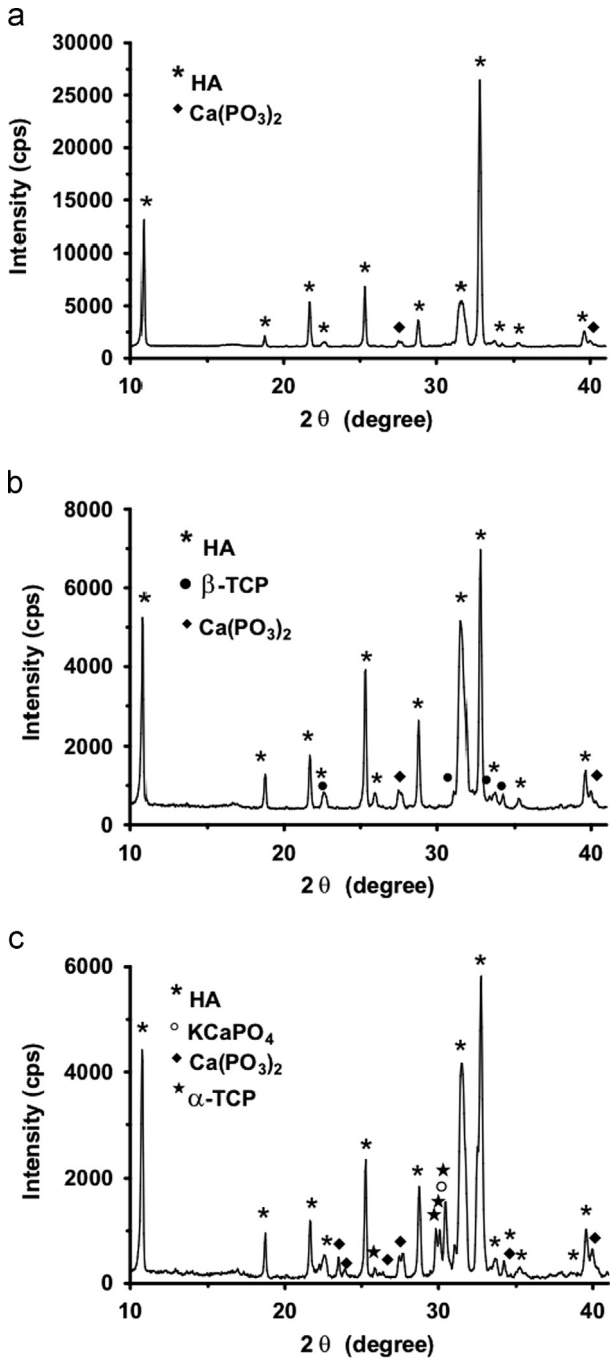


**Fig. 2.** XRD graphs show HA as the major phase of for all flux conditions along with minor phases for (a) HA:$K_2SO_4$ (1:3), (b) HA:$K_2SO_4$ (1:6), and (c) HA:$K_2SO_4$ (1:9).

198.5 AU, while 1:6 particles had a mean fluorescence of 174.2 AU, with the means being significantly different ($p=0.015$). The data suggest that increased molten $K_2SO_4$ content decreases the resultant bioceramic microparticles' capability to adsorb BSA-TRITC (Fig. 3b).

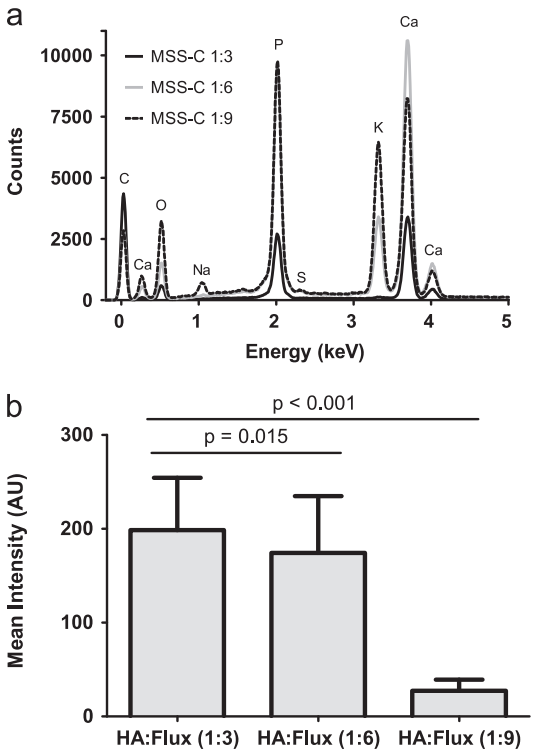


**Fig. 3.** (a) EDS indicates that Ca/P and Ca/K ratios decrease as HA:Flux ratios increase. (b) BSA-TRITC adsorption onto microparticles measured by mean fluorescence intensity of individual particles normalized to the imaged particle area using ImageJ. Non-parametric two-tailed student $t$-test (below $\alpha$-level 0.05 was significant, $n=70$ per group).

Although the 1:9 particles have a higher SSA and a similar zeta potential as the 1:6 particles, BSA adsorption is 6-fold higher on the 1:6 particles (Table 1). Therefore, the difference in protein adsorption cannot be explained solely based on the particles' zeta potential and SSA, but may be influenced by other material characteristics. Whether the change in protein adsorption is a direct effect of the substitution of potassium for calcium in the composite bioceramic, or the presence of minor orthophosphate phases, or the difference in morphology, needs further investigation.

## 4. Conclusions

Spheroidal potassium-substituted bioceramic microparticles were produced by molten salt synthesis and predominantly comprised of HA crystals grown along the $c$ axis. Potassium incorporation was apparent from a decreasing Ca/K molar ratio at higher $K_2SO_4$ content. With the increase of flux-to-HA ratio, the resultant particles were increasingly of spheroidal morphology. The adsorption of negatively charged BSA on the different microparticle batches was investigated. BSA adsorption decreased with higher potassium content and could not be predicted based on zeta potential and SSA alone. Highest BSA

adsorption was observed for the HA:$K_2SO_4$ (1:3) condition and was 7-fold higher compared to (1:9).

## Acknowledgments

The authors gratefully acknowledge the Oxford Martin School, the Department of Paediatrics and the Biomedical Ultrasonics, Biotherapy & Biopharmaceuticals Laboratory at the University of Oxford for the generous funding. The authors would also like to thank Dr P. Holdway (Oxford Materials Characterisation Service) for his assistance with X-ray diffraction.

## References

[1] Cormack AN, Tilocca A. Structure and biological activity of glasses and ceramics. Philos Transact A Math Phys Eng Sci 2012;370:1271–80.
[2] Fujii E, Ohkubo M, Tsuru K, Hayakawa S, Osaka A, Kawabata K, et al. Selective protein adsorption property and characterization of nano-crystalline zinc-containing hydroxyapatite. Acta Biomater 2006;2:69–74.
[3] Keselowsky BG, Collard DM, Garcia AJ. Integrin binding specificity regulates biomaterial surface chemistry effects on cell differentiation. Proc Natl Acad Sci USA 2005;102:5953–7.
[4] Hench LL. Bioceramics - from concept to clinic. Am Ceram Soc Bull 1993;72:93–8.
[5] Vasile E, Popescu LM, Piticescu RM, Burlacu A, Buruiana T. Physico-chemical and biocompatible properties of hydroxyapatite based composites prepared by an innovative synthesis route. Mater Lett 2012;79:85–8.
[6] Zhuang Z, Aizawa M. Protein adsorption on single-crystal hydroxyapatite particles with preferred orientation to a(b)- and c-axes. J Mater Sci Mater Med 2013;24:1211–6.
[7] Kandori K, Toshima S, Wakamura M, Fukusumi M, Morisada Y. Effects of modification of calcium hydroxyapatites by trivalent metal ions on the protein adsorption behavior. J Phys Chem B 2010;114:2399–404.
[8] Tas AC. Molten salt synthesis of calcium hydroxyapatite whiskers. J Am Ceram Soc 2001;84:295–300.
[9] Kimura T. Molten salt synthesis of ceramic powders. In: Sikalidis PC, editor. Advances in Ceramics - Synthesis and Characterization, Processing and Specific Applications. Shanghai: InTech; 2011.
[10] Tas AC. X-ray diffraction data for flux-grown calcium hydroxyapatite whiskers. Powder Diffr 2001;16:102–6.
[11] El Kady AA, Mohamed KR, El-Bassyouni GT. Fabrication, characterization and bioactivity evaluation of calcium pyrophosphate/polymeric biocomposites. Ceram Int 2009;35:2933–42.
[12] Augustine R, Kalappura UG, Laheurte JM, Mathew KT. Biocompatibility study of beta tricalcium phosphate bioceramics and chitosan biopolymer and their use as phantoms for medical imaging applications. Microw Opt Technol Let 2009;51:2923–7.
[13] Tomazic BB, Mayer I, Brown WE. Ion incorporation into octacalcium phosphate hydrolyzates. J Cryst Growth 1991;108:670–82.
[14] Zhang HG, Zhu Q. Preparation of fluoride-substituted hydroxyapatite by a molten salt synthesis route. J Mater Sci Mater Med 2006;17:691–5.